A comparative examination of the potential of screw expanders with variable rotor pitch

M. Utri, A. Brümmer
Chair of Fluidics, TU Dortmund University, Dortmund

Abstract

This paper contains a theoretical thermodynamic comparison of screw expanders with uniform and non-uniform pitch when deployed in an organic Rankine cycle system. In order to reveal the potential of a screw expander with variable rotor pitch, the optimized machine geometry with a uniform rotor pitch is first determined. Afterwards simulation is performed for rotor geometries consisting of two parts with different rotor pitch. Efficiency can be improved, especially in high pressure applications, caused by an optimized filling of the working chamber. The thermodynamic simulation is performed with the simulation tool KaSim, that calculates the fluid states inside the machines based on a multi-chamber model. The different machine versions are compared for constant fluid state at the inlet and are scaled under consideration of geometric similarity so as to ensure constant mass flow.

1 Introduction

Screw expanders are found in decentralised energy systems due to their high potential for energy conversion in lower and medium power ranges. A major geometric parameter of these machines is the wrap angle, which highly influences the size of the inlet opening area and the clearance situation of the machine. Due to manufacturing restrictions the rotors of screw machines are usually built with uniform rotor pitch, whereas variable pitch is already used in screw vacuum pumps and leads to improved energy efficiency.

Increased environmental awareness, and rising prices of primary energy, demand greater efficiency from technical systems. Exhaust heat recovery is one possibility to enhance power output of thermal processes, a technique which is already applied in higher power ranges like combined cycle plants, where the higher temperature exhaust heat of gas turbines is used in a Clausius Rankine cycle to vaporise water for steam turbines. New attempts to use exhaust heat from internal combustion engines in the lower and medium power range offer potential for screw expanders based on their high ability to convert energy and their performance under part-load conditions [1]. Regarding the working fluid, screw expanders do not require a

special purity or a superheated medium. This offers a range of application not accessible to other types of expander such as thermal turbomachinery. Screw expanders are highly suitable for application in organic Rankine systems that use an organic fluid instead of water. The lower boiling point of these fluids is advantageous for cycles that operate at a noticeably lower temperature level.

2 Working principle of screw expanders

The working cycle and the main parameters of screw expanders will be explained by referring to the pressure-volume diagram shown in **Fig. 1**. The working cycle can be sectioned in three phases. During the charging phase (phase 1), the emerging working chamber of the expander is filled with a fluid through the inlet opening area. During the expansion phase (phase 2), the working chamber is almost closed and only interacts with other chambers and machine ports due to clearance mass flows. The pressure drops, caused by an increase in chamber volume. As maximum volume is reached, the discharge phase begins and the chamber becomes connected to the low pressure port via the outlet area (phase 3).

The pressure level inside the working chamber during the charging progress is mainly influenced by three effects:

- Increase of pressure due to inlet fluid flow when the high pressure port opens. Mass flow is limited by the available opening area and the fluid states on the high pressure side and inside the working chamber.
- Decrease of pressure due to continuously increasing chamber volume.
- Decrease of pressure due to clearance mass flows. The clearance area increases during the charging progress.

The intensity of these effects is highly dependent on the rotational speed and the geometrical parameters of the expander, such as the length to diameter ratio and the wrap angle φ_{MR}, which can be defined as the twisting between the front and the rear cross sections of the rotor. Assuming a given rotor diameter and profile, these parameters determine the volume curve and the inlet opening area of the expander. As shown in the indicator diagram, the pressure inside the working chamber never reaches the available high pressure conditions because of throttling effects. The higher the maximum chamber pressure, the more expansion work can be achieved during expansion. The pressure decreases rapidly prior to reaching the high pressure control edges, although the chamber is still being filled through the inlet opening area.

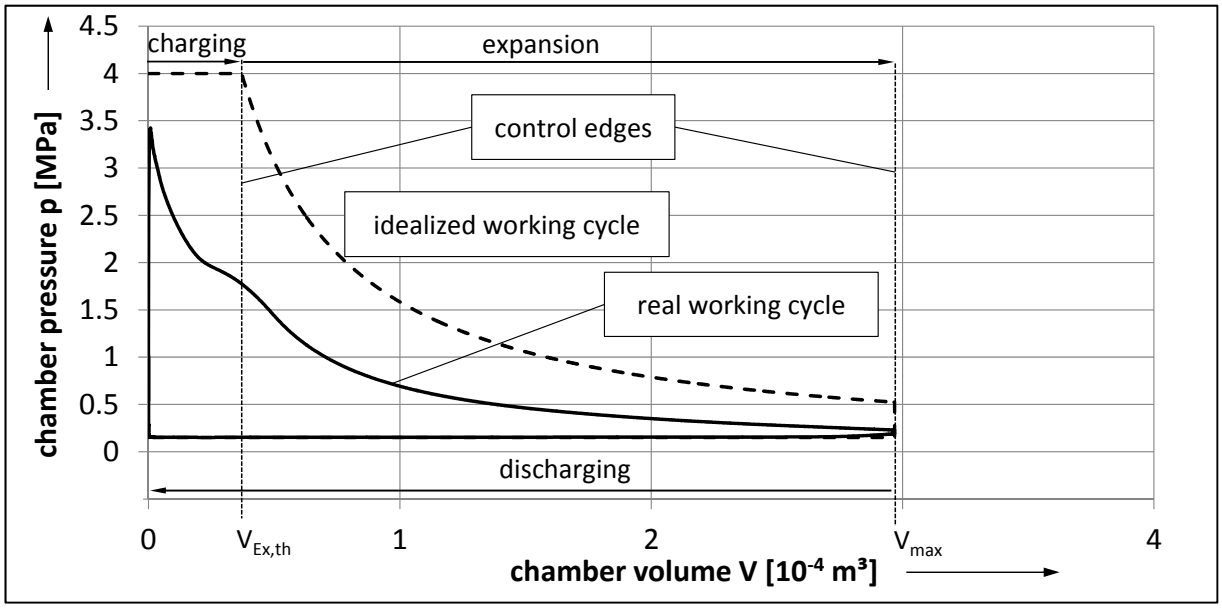

Fig. 1 Pressure-volume diagram of a real and idealized working cycle.

The positions of the control edges in the machine housing determine the internal volume ratio v_i, which is defined as the ratio between the maximum chamber volume at the end of expansion V_{max} and the volume at the theoretical start of expansion $V_{Ex,th}$, equation 1.

$$v_i = \frac{V_{max}}{V_{Ex,th}} \tag{1}$$

Adjusting the control edges towards lower rotor rotation angles α_{MR} reduces chamber volume at the theoretical start of expansion, thereby increasing the internal volume ratio and shortening the charging phase. This influences the pressure change in the working chamber as well as the pressure at the end of expansion and the expander mass flow and therewith the power output of the expander. A cycle with an expansion that ends exactly at the level of the low pressure port is called an adapted working cycle. The expander's energetic efficiency can be quantified by the effective isentropic efficiency, that is the ratio of the useable expander power $P_{e,exp}$ and the enthalpy flow $\Delta\dot{H}_s$ assuming an isentropic expansion from high pressure to low pressure conditions:

$$\eta_{e,s} = \frac{P_{e,exp}}{\Delta\dot{H}_s} \tag{2}$$

3 Multi-Chamber Simulation

To determine the operating behaviour of screw expanders, multi-chamber simulation is performed as described in detail in [2]. This method is based on mass and energy conservation and considers the periodic behaviour of positive displacement machines. The

geometry of the screw machine is abstracted to a zero dimensional model that includes chamber volumes and ports (“capacities”) as well as opening areas and clearances (“connections”) as a function of the rotor position α_{MR}. This geometrical abstraction is presented in detail in [3]. The fluid state in the capacities is assumed to be homogeneous. During simulation, a time-dependent mass flow between the capacities is calculated that depends on the fluid state of the connected volumes and the available area and geometry of the connection. In the case of adiabatic and frictionless flow, the exchanged mass flow can be calculated by equation 3, where index 0 is the volume with the higher pressure and pressure ratio is subcritical [2].

$$\dot{m}_{th} = A \cdot p_0 \cdot \sqrt{\frac{2\kappa}{(\kappa-1)\cdot R \cdot T_0}} \cdot \sqrt{\left(\frac{p_1}{p_0}\right)^{\frac{2}{\kappa}} - \left(\frac{p_1}{p_0}\right)^{\frac{\kappa+1}{\kappa}}} \tag{3}$$

Considering flow involving friction, the exchanged theoretical mass flow is reduced by what is defined as the friction coefficient α when:

$$\dot{m} = \alpha \cdot \dot{m}_{th} \tag{4}$$

According to Dreißig [4] the friction coefficient is set to $\alpha = 0.8$ for all clearances and opening areas. While flowing into the working chambers, the fluid needs to be accelerated to the circumferential speed of the screw expander. Assuming this motion energy will dissipate when the fluid is pushed to the low pressure port, this loss is estimated with

$$P_c = \dot{m}_{ORC} \cdot \frac{u_{MR}^2}{2} \tag{5}$$

in which u_{MR} is the male rotor tip speed and $\dot{m}_{ORC}$ is the inlet mass flow of the expander. The results of the simulation contain, amongst others, the indicator diagram of the simulated machine, the internal expander power and the expander mass flow.

4 Exhaust heat recovery with ORC

The purpose of an organic Rankine cycle (ORC) system is to convert thermal energy, in this case, the heat recoverable from an IC engine exhaust gas, into mechanical work. A feed pump moves the liquid fluid to a feed heater and vaporiser, where heat flows from the exhaust gas to the working fluid and the fluid state changes from liquid to vapour after reaching its local boiling point. Subsequently the vapour flows through an expansion machine

and the fluid energy is converted to shaft work. Afterwards the fluid flows through a condenser, where it is returned to the liquid phase, before re-entering the feed pump.

The ORC mass flow depends on the exchanged input heat flow $\dot{Q}_{in}$ and the enthalpy increase that is necessary for feed heating and vaporisation of the working fluid, as shown in equation 6. Assuming that there are no heat losses within the ORC, this enthalpy difference is described between the fluid states after flowing out of the feed pump $h_{out,p}$ and before entering the expander $h_{in,exp}$.

$$\dot{m}_{ORC} = \frac{\dot{Q}_{in}}{h_{in,exp}-h_{out,p}} \tag{6}$$

Equation 7 defines the thermal efficiency η_{th} of the ORC. The net output of the ORC system is the effective expander power minus the input power to the feed pump, whereas the effective efficiency of the feed pump is assumed to be $\eta_{e,p} = 0.8$ in all simulations. The heat input is the overall heat flow supplied by the exhaust gas.

$$\eta_{th} = \frac{P_{ORC}}{\dot{Q}_{exh}} = \frac{P_{e,exp}-P_{e,p}}{\dot{Q}_{exh}} \tag{7}$$

In contrast to the isentropic efficiency of the expander, the thermal efficiency quantifies the efficiency of the whole Rankine cycle, not just of the expansion process. Optimization of the isentropic efficiency does not imply an optimized ORC system [5].

5 Boundary conditions and machine scaling

The parameters of the ORC system are determined assuming constant operation of a ship's combustion engine. This creates a mass flow of exhaust gas $\dot{m}_{exh} \approx 1.8$ kg·s^{-1} at a temperature of $T_{exh} \approx 650$ K. The exhaust gas is a mixture of nitrogen, carbon dioxide and water and leads to a maximum heat flow of $\dot{Q}_{exh} \approx 570$ kW assuming an exit temperature level of 373 K from the ORC boiler. The working fluid of the cycle is ethanol. A superheated ORC is possible, but former investigation indicated that the ORC system reaches its maximum power output when operated with saturated vapour [5]. Simulations are carried out for three different expander inlet pressures $p_{in,exp}$ as shown in **table 1**, while the discharge pressure at the expander outlet is set at a constant value of $p_{out,exp} = 0.15$ MPa.

The examined machine is an oil free GL51 type screw expander with three male and five female rotor teeth. The rotor profile is based on the classical asymmetric SRM profile, which is modified in order to reduce abrasion in case of non-synchronized application [2].

To ensure that the expander always delivers the pressure depending ORC mass flow, as shown in table 1, the machine geometry for each selected circumferential speed or geometric parameter is scaled under consideration of full geometrical similarity (including clearance heights) during simulation at constant circumferential speed. This affects both the dimensions of the simulated machine and its rotational speed. In addition to thermodynamic behaviour, this also influences the mechanical efficiency η_m of the simulated machine, which takes into consideration friction in bearings and seals and decreases the useable expander power output. According to the investigations of von Unwerth [6] mechanical efficiency is considered to degrade linearly with rotational speed and is set to $\eta_m = 0.9$ at a rotational speed of $n_{MR} = 20\,000\ min^{-1}$.

Clearance heights of the unscaled machine are set to 0.1 mm for the front, 0.08 mm for the housing and a middle profile clearance height of 0.05 mm for a male rotor diameter of $D_{MR} = 72$ mm. The examined length to diameter ratio of the male rotor is set to $D_{MR}/L_{MR} = 1.4$, leading to a length of $L_{MR} = 100$ mm. Furthermore, all simulations are carried out without any heat exchange between the working fluid and surrounding machine parts.

Table 1: Properties of the ORC mass flow for saturated ethanol vapour

expander inlet pressure [MPa]	expander inlet temperature [K]	ORC mass flow [kg/s]
1	424	0.611
2	454	0.599
4	489	0.601

6 Variation of internal volume ratio

In order to determine the most advantageous expander geometry with a constant rotor pitch for the given ORC parameters, the expander geometry is varied systematically. The operational behaviour of screw expanders is highly influenced by the rotational speed of the rotors. Circumferential speed is varied in order to find the energetic optimum of the simulated machine, each again scaled to the predefined mass flow.

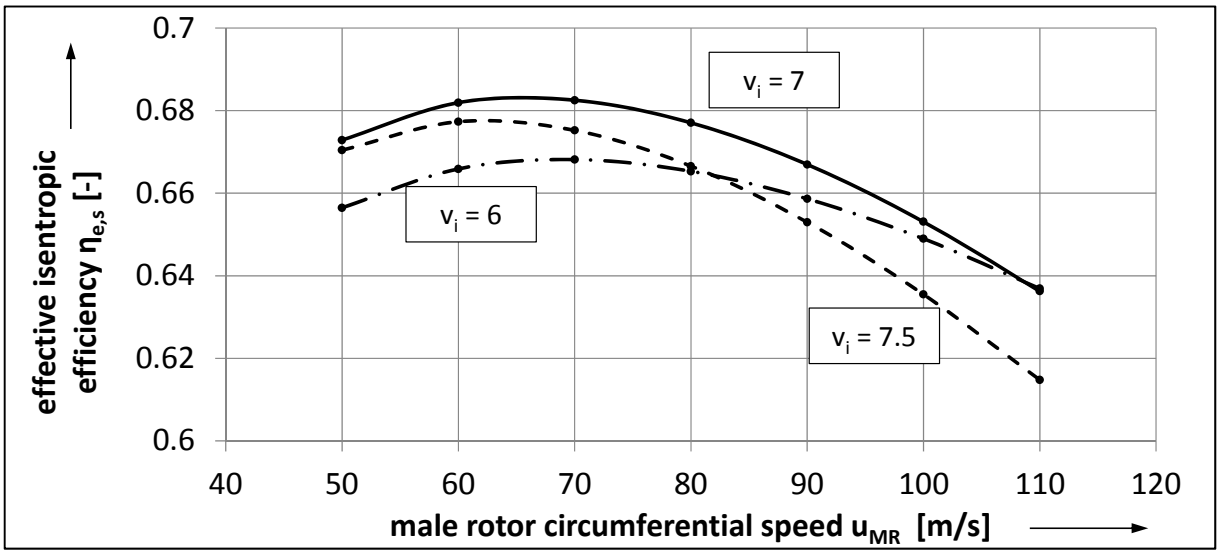

Fig. 2 Effective isentropic efficiency as a function of male rotor circumferential speed for $p_{in,exp}$ = 4 MPa and φ_{MR} = 400°. Each point represents a machine scaled to a constant mass flow of $\dot{m}_{ORC}$ = 0.601 kg·s^{-1}.

Fig. 2 shows the results of varying the internal volume ratio and circumferential speed while the wrap angle, length to diameter ratio and inlet and outlet conditions remain constant. Assuming a constant machine geometry, a change in the internal volume ratio affects the size of the inlet opening area and thereby the mass flow of the screw expander by varying the duration of the charging progress. Thus, the machine geometry is scaled during simulation to ensure the boundary of a constant ORC mass flow. Geometrically similar up-scaling causes a cubic increase of the displaced volume, while rotational speed is varied to maintain the requirement of constant circumferential speed. In contrast, an increase of circumferential speed causes smaller machine geometries and increased rotational speeds. This leads to a decrease in the clearance mass flows per working cycle, but also amplifies the losses due to mechanical friction as well as acceleration of the fluid and throttling of the inlet mass flow.

At constant circumferential speed, machines with higher internal volume ratios require enlarged geometry dimensions, but smaller inlet areas and lower rotational speeds because of the scaling process described above. For this reason, the absolute maximum of efficiency at an internal volume ratio of seven and a circumferential speed of u_{MR} = 70 m/s is not achieved in an adapted working cycle. The highest efficiency achieved is for an expansion that ends at a higher pressure level compared to the low pressure conditions because an increase of the internal volume ratio strongly enlarges the machine dimensions and thereby internal leakage caused by the lower rotational speed.

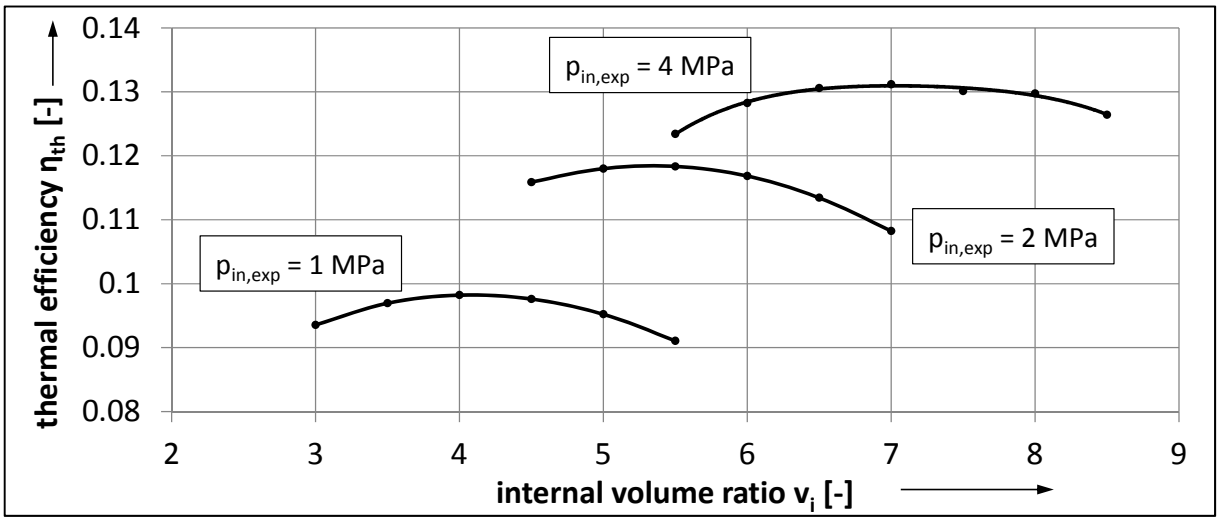

Fig. 3 Thermal efficiency as a function of internal volume ratio for φ_{MR} = 400° for optimal circumferential speed. Each point represents a machine scaled to a constant mass flow as shown in table 1.

To evaluate the overall efficiency of the ORC system, **Fig. 3** shows how the thermal efficiency varies with changes in the expander inlet pressure and the internal volume ratio. Only peak values of the variation of circumferential speed are presented for each internal volume ratio. The cycle efficiency increases when operating at higher pressures due to the higher evaporation temperatures with which they are associated. This, in turn, leads to an increase in the maximum possible efficiency of the cycle [7].

7 Variation of constant rotor wrap angle

The wrap angle of the rotors is the major geometric parameter that will be discussed in this article. **Fig. 4** clarifies the influence of the wrap angle on the volume curve considering the boundary of constant rotor diameter and length. An increase in wrap angle reduces the gradient of the volume curve while increasing the duration of the working cycle. Furthermore, the maximum chamber volume decreases significantly for wrap angles greater than φ_{MR} = 245°. In the boundaries examined, wrap angles greater than φ_{MR} = 200° cause lobe engagement of the male rotor at the downside of the high pressure intersection, before the rotor lobes disengage completely at the upside of the low pressure intersection, as shown in **Fig. 5**. Thus the chamber volume on the male rotor side remains constant, while the chamber volume on the female rotor side still increases. This can be seen, for example, in the change of gradient in the linear phase of the volume curve for male rotor wrap angles of 500° and 600°. For wrap angles of 300° and 400° this effect cannot be seen in the diagram because lobe engagement takes place during the regressive phase of the volume curve. Besides the decrease of maxi-

mum chamber volume, lobe engagement causes a harmful bypass to the leading working chamber which is already opened to the low pressure port. In order to obey the requirement of constant ORC mass flow, machines with higher wrap angles show greater geometry dimensions and decreased rotational speeds due to the scaling process. Combined with the longer duration of the working cycle itself, this causes raised clearance mass flows.

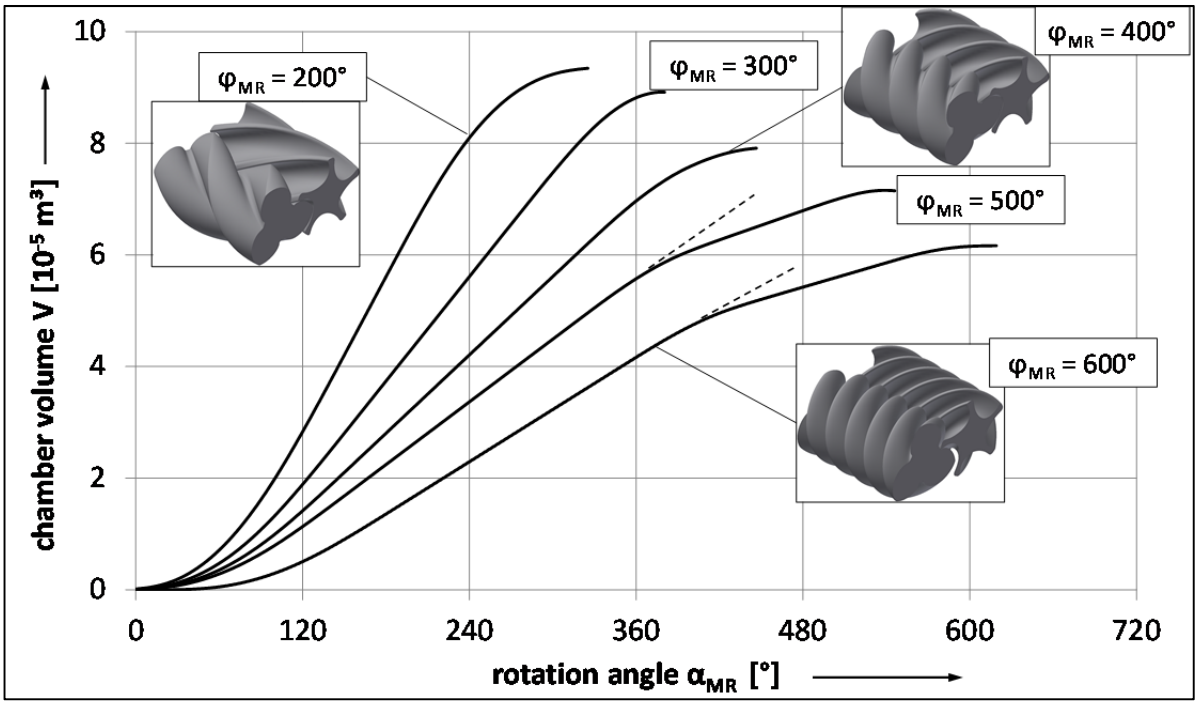

Fig. 4 Volume curves for different male rotor wrap angles (D_{MR} = 72 mm, L_{MR} = 100 mm).

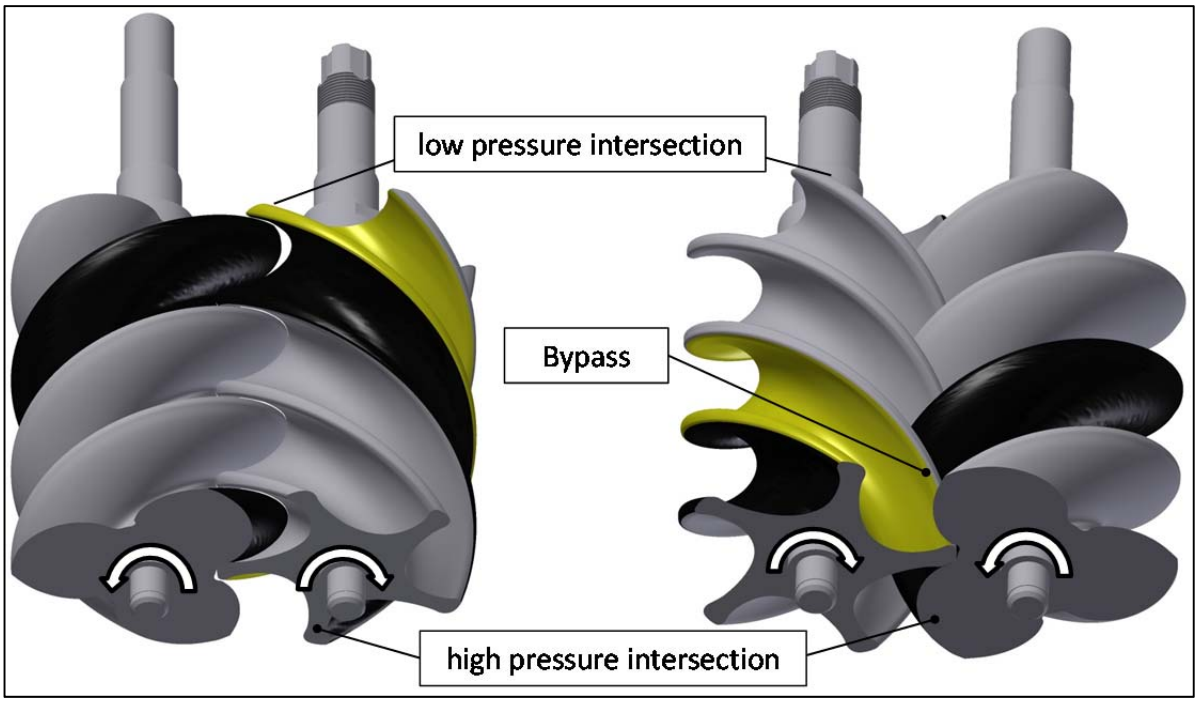

Fig. 5 Exemplary view of the expander upside (left) and downside (right) for φ_{MR} = 400°.

Fig. 6 shows how thermal efficiency varies with the wrap angle. The results shown always represent the internal volume ratio and circumferential speed dependent optimum of the examined machine version. On the one hand, small wrap angles offer advantageous reduced clearance areas; on the other hand, they show small inlet opening areas due to rapidly increasing chamber volume. Machines with a higher wrap angle instead show enlarged clearance areas but offer a big inlet opening area combined with a moderate increase in chamber volume, that leads to improved filling. For wrap angles higher than 400°, the working chamber reaches its maximum volume before reaching the low pressure intersection due to lobe engagement at the expander downside that takes place on the male and female rotor side. Thus the rotor length remains partly unused for energy conversion and, together with larger clearance areas, causes a decrease in thermal efficiency. Examination of the indicator diagrams (not shown) reveals strong throttling effects for a wrap angle of 200°, but a flat expansion progression due to small clearances and fast growth in chamber volume. This provides little time for clearance mass flows. For wrap angles higher than 400° chamber filling no longer improves, but pressure in the working chamber drops with a higher gradient due to the large clearance areas and a long working cycle.

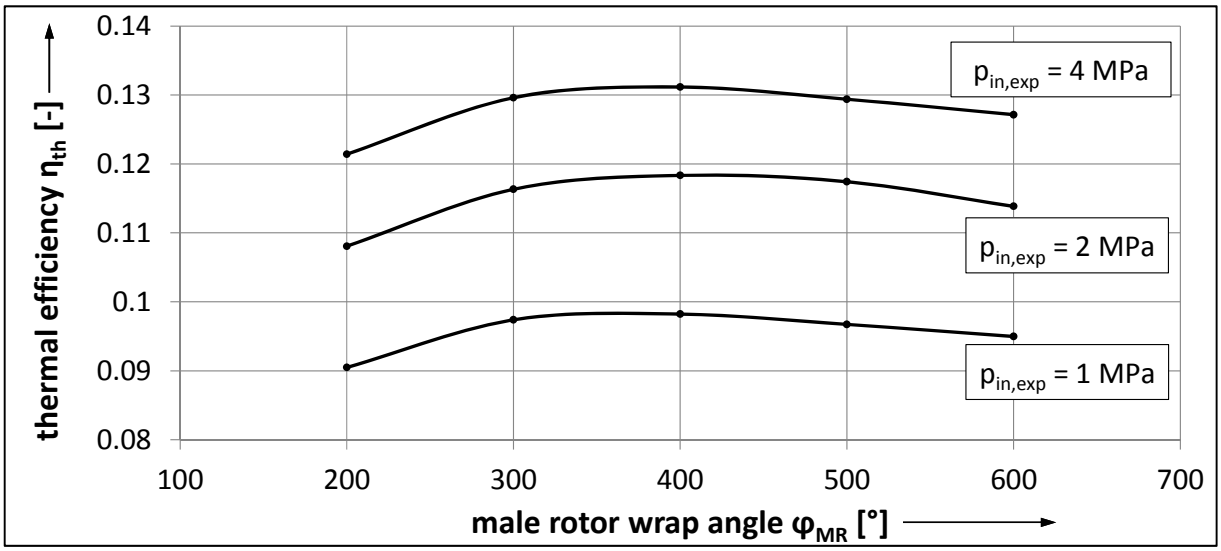

Fig. 6 Thermal efficiency as a function of male rotor wrap angle. Each point represents a machine scaled to a constant mass flow as shown in table 1.

Fig. 7 shows the pressure-volume diagrams for the optimal male rotor wrap angle φ_{MR} = 400°. For an inlet pressure of $p_{in,exp}$ = 1 MPa chamber filling is almost isobaric. An increase in the inlet pressure leads to higher pressure ratios and, in combination with the higher internal volume ratio, to strong throttling effects. For $p_{in,exp}$ = 4 MPa the chamber pressure never reaches the expander inlet pressure conditions and expansion starts early

prior to reaching the high pressure control edges, meaning that the potential pressure offered is underachieved. This leaves potential for optimization of the chamber filling to enhance the ORC power output because the maximum power output may be expected for high pressure applications as illustrated in Figs. 3 and 6.

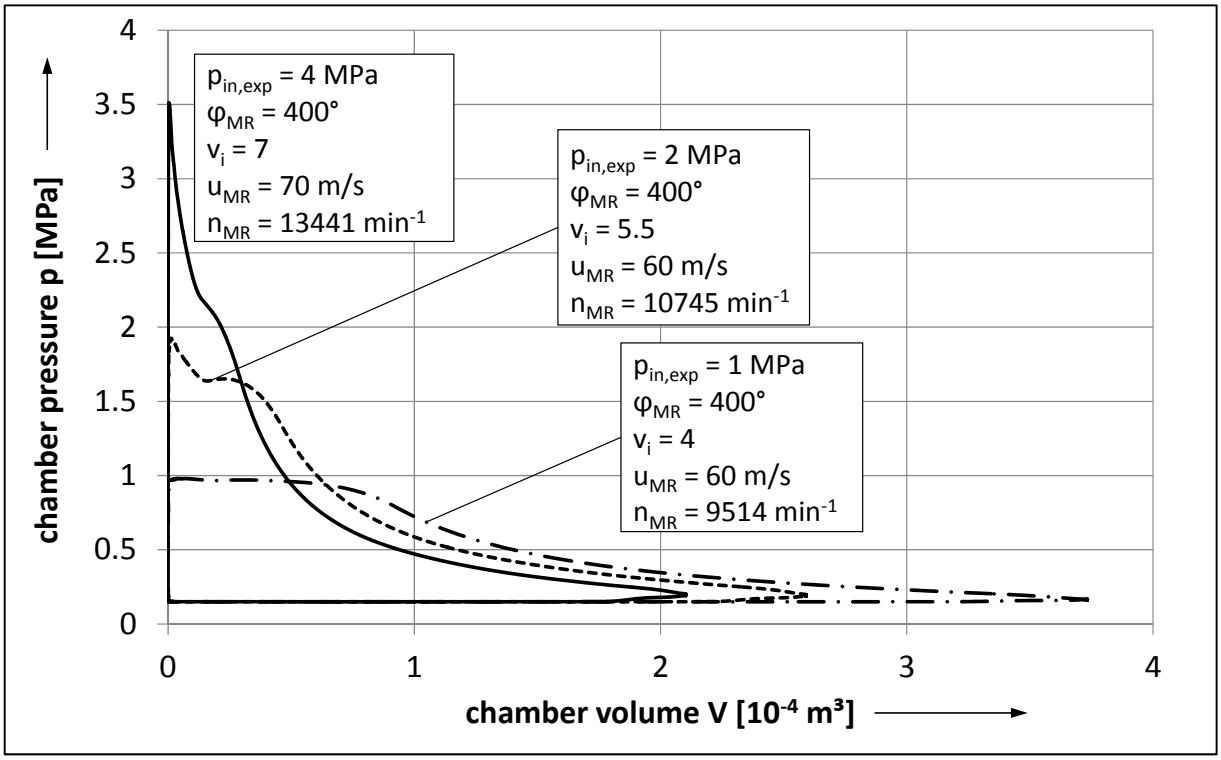

Fig. 7 Indicator diagrams for optimized expander geometries with constant wrap angle φ_{MR} = 400° for three different inlet pressures and optimal internal volume ratios.

8 Variable rotor pitch

A screw expander with variable pitch offers the possibility to combine the advantages of small and big wrap angles in one machine as previously discussed. Parameters like length to diameter ratio are held constant as shown in the examination of constant rotor pitch. Within the scope of the investigation are rotors with two different wrap angles as shown in **Fig. 8**, providing three parameters that can be adjusted: The overall wrap angle of the whole rotor φ_{MR}, defined as the twisting between the front and the rear surface of the rotor, and the wrap angles φ_1 and φ_2 of the rotor sections L_1 and L_2. Like the overall wrap angle φ_{MR} the wrap angles φ_1 and φ_2 are also specified referring to the whole rotor length L_{MR} as shown in Fig. 8. Thus the parameters of the rotor are dependent as shown in equation 8 and 9.

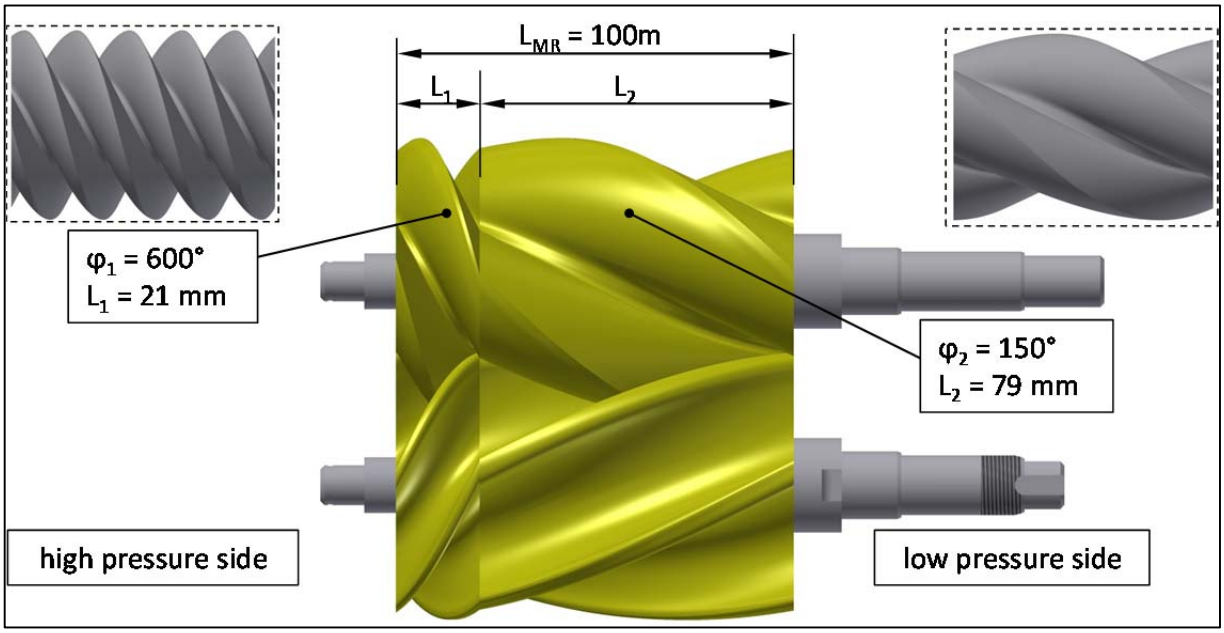

Fig. 8 Geometry of a screw expander with two different rotor pitches on one rotor for an overall wrap angle of φ_{MR} = 245°.

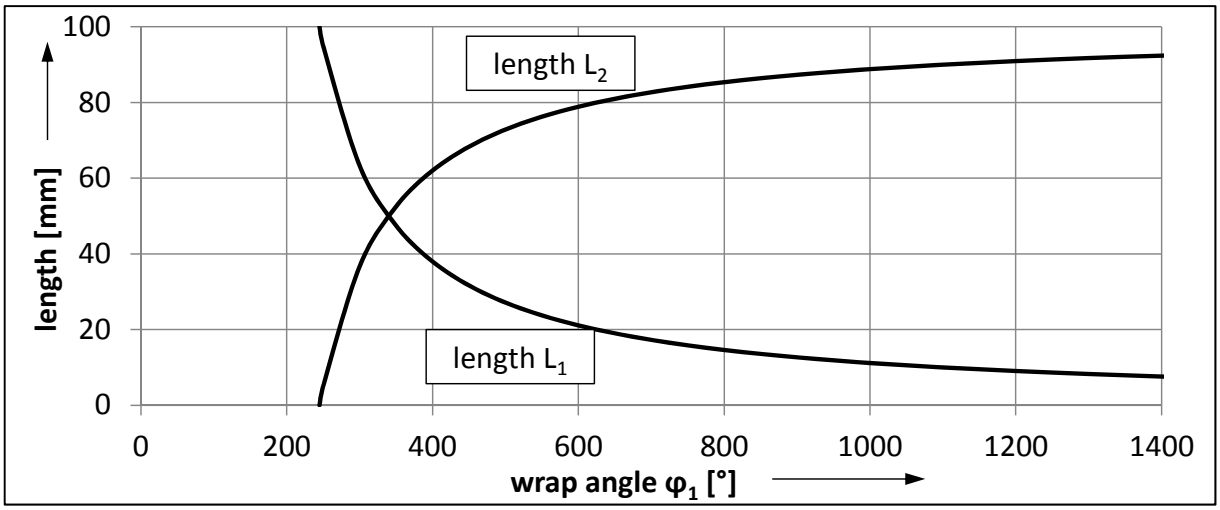

Fig. 9 Lengths L_1 and L_2 as a function of wrap angle φ_1 for an overall wrap angle of φ_{MR} = 245°, a wrap angle of φ_2 = 150° in section L_2 and an overall length of L_{MR} = 100 mm

$$L_{MR} \cdot \varphi_{MR} = L_1 \cdot \varphi_1 + L_2 \cdot \varphi_2 \quad (8)$$

$$L_{MR} = L_1 + L_2 \quad (9)$$

These equations lead to a typical distribution of the wrap angle sections, shown in **Fig. 9**. The wrap angle φ_1 on the high pressure side is varied while the overall length L_{MR} and the wrap angles φ_2 and φ_{MR} remain constant as illustrated in Fig. 8. Section L_1 decreases

regressively for a linear increase of wrap angle φ_1. Due to the boundary of a constant overall length, the low pressure section L_2 increases correspondingly.

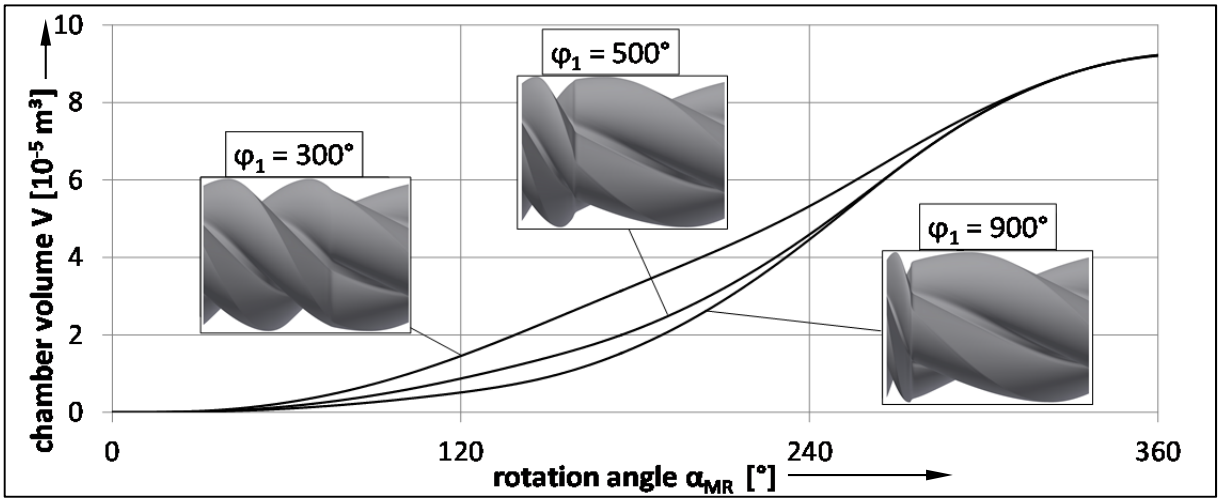

Fig. 10 Volume curves for a variation of the male rotor wrap angle φ_1 for D_{MR} = 72 mm, L = 100mm, φ_{MR} = 245° and φ_2 = 150°.

Fig. 10 shows the corresponding volume curves for variation in wrap angle φ_1. The overall wrap angle φ_{MR} represents the crucial parameter for the displaced chamber volume and the duration of the working cycle. For this reason, this article concentrates on wrap angle parameter instead of rotor pitch. For a constant length of L_{MR} = 100 mm before machine scaling, the set overall wrap angle defines the maximum chamber volume shown in Fig. 4. Fig. 10 demonstrates the possibility of influencing the volume curve without changing the maximum chamber volume. To improve the charging of the working chamber it is reasonable to equip the rotor with an enlarged wrap angle at the high pressure intersection side (length L_1) and a moderate wrap angle at the low pressure intersection side (length L_2). The higher the wrap angle on the high pressure side, the flatter is the progress at the beginning of the volume curve. While the working chamber is located in length L_1, an increase in chamber volume will be very moderate and lead to a large inlet opening area and a longer charging phase, but at the same time to an increasing clearance mass flow during the filling process. After reaching the lower wrap angle in length L_2, the chamber volume increases rapidly and maintains quick expansion of the fluid. Thus clearance mass flows during the expansion phase can be reduced and an enhanced efficiency of the expander may be expected.

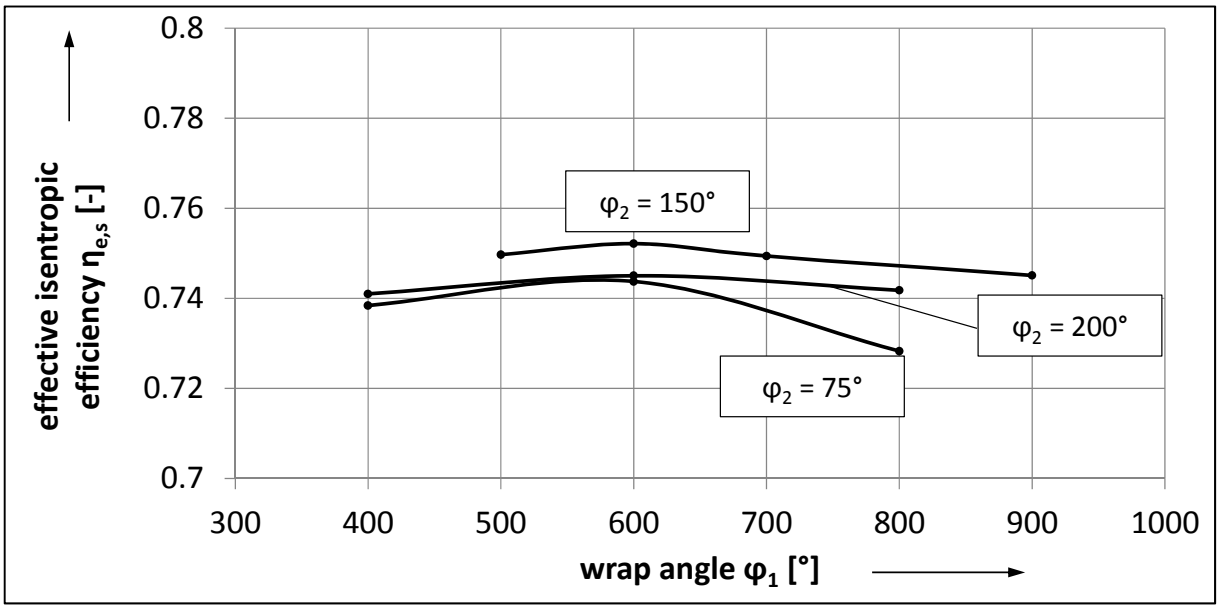

Fig. 11 Effective isentropic efficiency as a function of wrap angle φ_1 for an overall wrap angle of φ_{MR} = 245°, an optimal internal volume ratio and $p_{in,exp}$ = 2 MPa. Each point represents a machine scaled to a constant mass flow of $\dot{m}_{ORC}$ = 0.599 kg·s^{-1}.

Wrap angle parameters, circumferential speed and internal volume ratios have been varied widely and revealed the best geometry parameters. In the case of a high overall wrap angle φ_{MR}, maximum chamber volume decreases, leading to the disadvantages already discussed for uniform rotor pitch. Thus an overall wrap angle of φ_{MR} = 245° is most advantageous because chamber volume is maximized, as previously explained.

Fig. 11 shows the effective isentropic efficiency for varying the wrap angles φ_1 and φ_2. Only the internal volume ratio and circumferential speed dependent optima of the examined machine version are shown. A small wrap angle (φ_2 = 75°) on the low pressure side of the expander maintains a long section L_1 with the higher wrap angle φ_1. Thus the chamber increase is still located in section L_1 although the charging process is finished. This leads to a growth of clearance mass flows. A high wrap angle φ_2 = 200° causes slower expansion due to increased length L_2. The working chamber reaches section L_2 before the charging progress is finished, which worsens filling. For the given boundaries $p_{in,exp}$ = 2 MPa, an expander with a wrap angle of φ_1 = 600° on the high pressure side and φ_2 = 150° on the low pressure side reveals the best energy conversion. The working chamber reaches the lower wrap angle section exactly as the charging progress is completed.

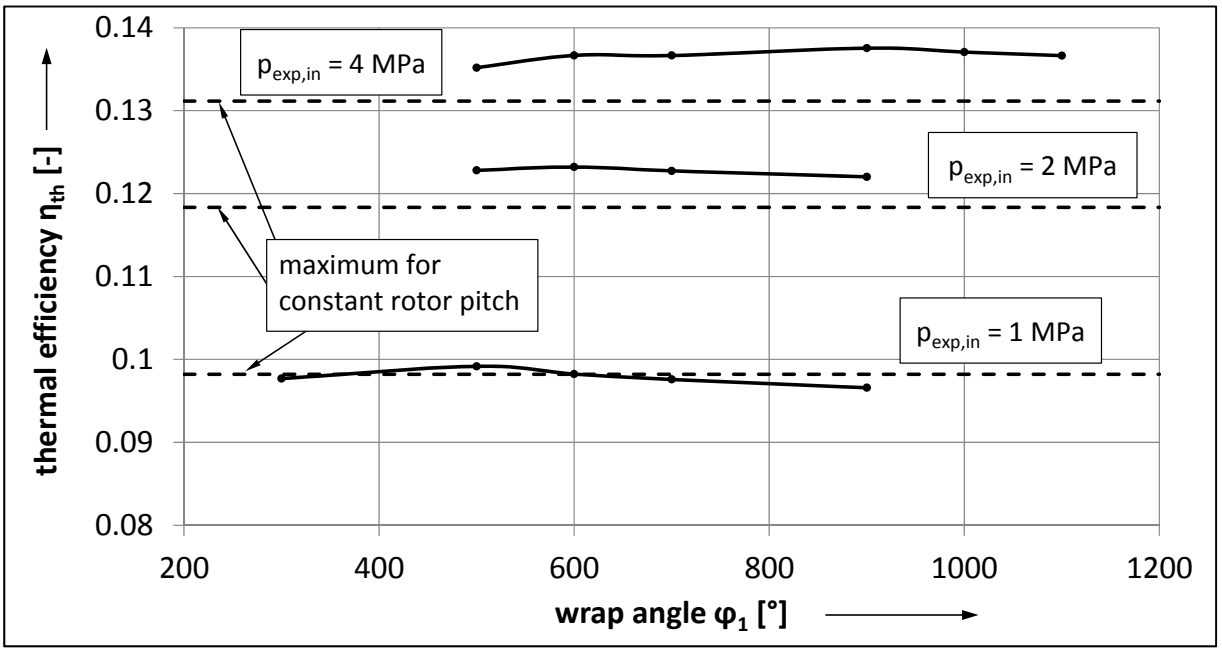

Fig. 12 Thermal efficiency as a function of wrap angle φ_1 for φ_2 = 150° and φ_{MR} = 245°. Each point represents a machine scaled to a constant mass flow as shown in table 1.

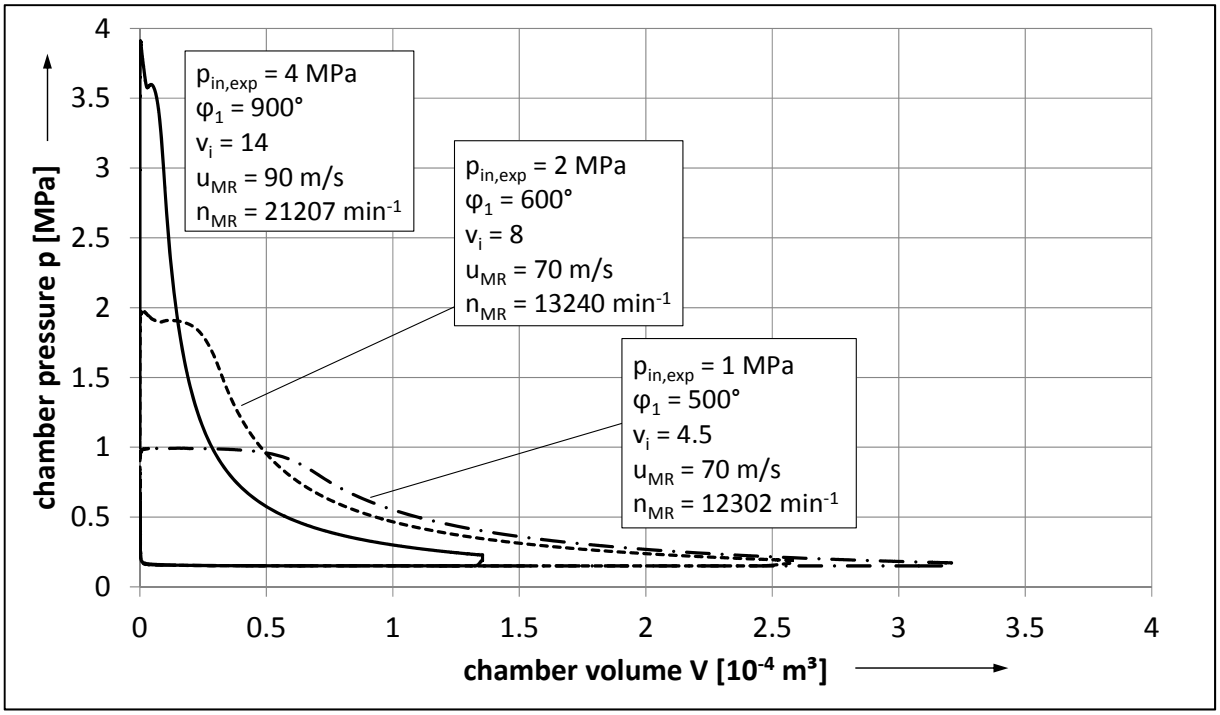

Fig. 13 Indicator diagrams for optimized expander geometries with variable wrap angles φ_{MR} = 245° and φ_2 = 150° for three different inlet pressures and optimal internal volume ratios.

Fig. 12 shows the development of thermal efficiency for an overall wrap angle of φ_{MR} = 245° and a wrap angle on the low pressure side of φ_2 = 150°. Fig. 7 already revealed that the

filling process is almost isobaric for an inlet pressure of $p_{exp,in}$ = 1 MPa. For this reason, variable rotor pitch causes only little improvement in efficiency. For higher inlet pressures the rotor configuration offers a remarkable increase in thermal efficiency due to an optimized filling process, which can also be seen in the corresponding indicator diagrams in **Fig. 13**. The optimal wrap angle φ_1, on the high pressure side, rises with higher inlet pressures because the reduced increase of chamber volume is advantageous to avoid throttling effects. As a result of improved chamber filling, maximum power output is achieved at higher circumferential speed and rotational speed and thereby leads to reduced internal leakage.

Fig. 14 shows the improvement that can be achieved for the high pressure conditions of 4 MPa. The available opening area for variable pitch is much greater than for constant pitch, although the internal volume ratio for variable pitch is higher. This is caused by the moderate increase in chamber volume during the filling for the expander with variable pitch. The greater inlet area leads to improved filling. Thus the machine is scaled to a smaller diameter, which reduces the clearance area, increases the rotational speed and improves the expander power output.

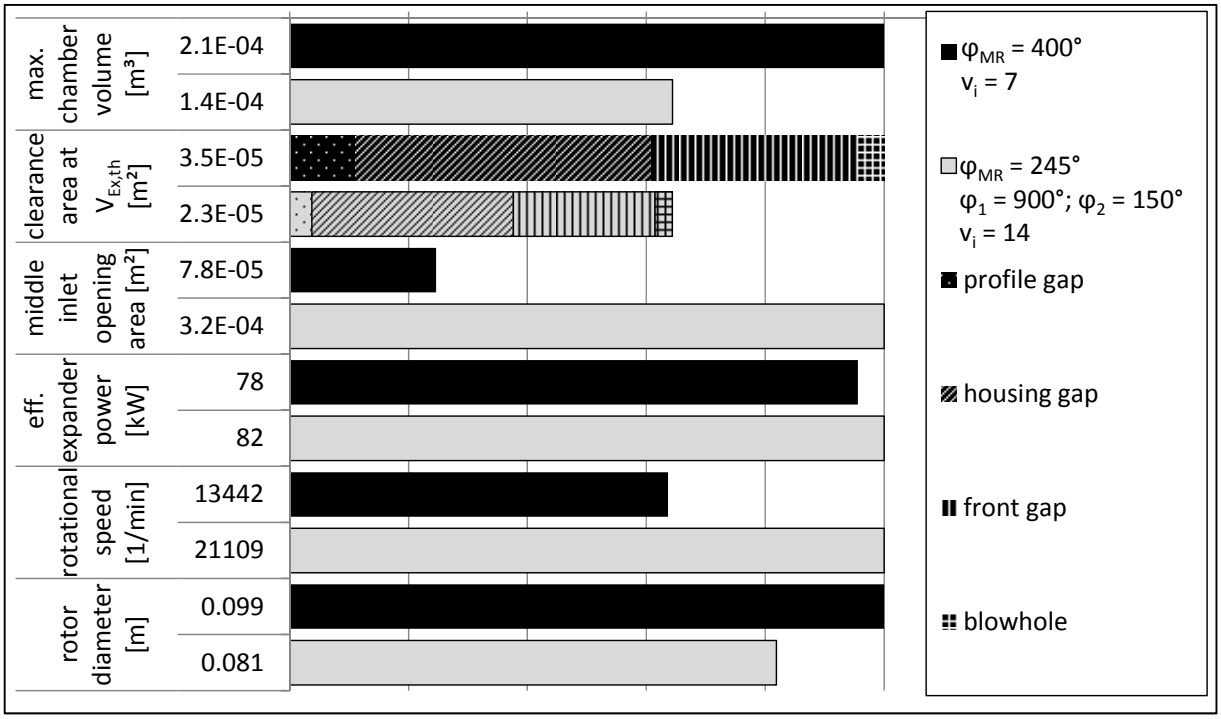

Fig. 14 Comparison of expanders with optimal constant rotor pitch (black) and variable rotor pitch (grey) for $p_{exp,in}$ = 4 MPa. Both machines scaled to a constant mass flow of $\dot{m}_{ORC}$ = 0.601 kg·s^{-1}.

9 Conclusion

This paper contains a theoretical thermodynamic comparison of screw expanders with uniform and variable rotor pitch applied to organic Rankine cycle systems. In order to determine possible advantages of varying the pitch, optimum machine geometries for constant pitch were first determined. For lower inlet pressures uniform rotor pitch delivers satisfactory results with an almost isobaric filling. For higher inlet pressures, which represent the more relevant operating points in organic Rankine cycle systems, heavy throttling effects occur. With variable rotor pitch, the charging process of the expander could be improved by a larger inlet opening area combined with an optimized progression of the volume curve. This leads to a smaller expander geometry and thus to less clearance areas. Expanders with variable rotor pitch provide up to an additional 5% in effective power output. This underlines their potential in the described fields of application. Optimal results are achieved when the growing working chamber reaches the rotor section with a higher rotor pitch at the theoretical start of expansion. Due to the challenging shape of the rotor surface, further examination should focus on the possibilities of manufacturing rotors with variable pitch. Furthermore, the influence of length to diameter ratio on the efficiency of expanders should also be investigated.

References

[1] Hütker, J., Brümmer, A.: Physics of a dry running unsynchronized twin screw expander. In: 8th International Conference on Compressors and their Systems (page 407 – 416), City University London (2013)

[2] Janicki, M.: Modellierung und Simulation von Rotationsverdrängermaschinen. Dissertation, TU Dortmund (2007)

[3] Nadler, K., Brümmer, A.: A method for the geometrical analysis of twin-shaft rotary displacement machines. VDI-Berichte Schraubenmaschinen (page 333 – 344), Springer Verlag (2010)

[4] Dreißig, B.: Ein Beitrag zur Auslegung von trockenlaufenden Schraubenmotoren. Dissertation, TU Dortmund (1989)

[5] Grieb, M., Brümmer, A.: Application-Oriented Design and Theoretical Investigation of a Screw-Type Steam Expander. In: International Compressor Conference, Purdue (2014)

[6] von Unwerth, T.: Experimentelle Verifikation eines Simulationssystems für eine GASSCREW. Dissertation, TU Dortmund (2002)

[7] Smith, I. K., Stosic, N., Kovacevic, A.: Power recover from low-grade heat by means of screw expanders. Woodhead Publishing (2014)

Symbol	Dimension	Meaning	Subscript	Meaning
$\dot{H}$	W	enthalpy flow	c	circumferential
h	$J \cdot kg^{-1}$	specific enthalpy	e	effective
L	m	length	exh	exhaust gas
$\dot{m}$	$kg \cdot s^{-1}$	mass flow	exp	expander
n	min^{-1}	rotational speed	Ex,th	theoretical start of expansion
P	W	power	in	expander inlet condition,
p	Pa	pressure		incoming heat flow
$\dot{Q}$	W	heat flow	m	mechanical
R	$J \cdot kg^{-1} \cdot K^{-1}$	gas constant	max	maximum
T	K	temperature	MR	male rotor
u	$m \cdot s^{-1}$	circumferential speed	ORC	organic Rankine cycle
V	m^3	volume	out	expander outlet condition
v_i	-	internal volume ratio	p	pump
α	°	rotation angle	s	isentropic
α	-	friction coefficient	th	thermal, theoretical
Δ	-	difference	v	vaporiser
η	-	efficiency	0, 1	fluid states
κ	-	isentropic exponent	1, 2	rotor sections
φ	°	wrap angle		